KAPITEL 2 / *CHAPTER 2* [2]
QUARTZ PULSE WAVE SENSOR WITH A CAPACITIVE CONTROL FOR HEALTHCARE SOLUTIONS

DOI: 10.30890/2709-2313.2024-29-00-031

Introduction

This chapter describes the design principles of a quartz pulse wave sensor with capacitive control for healthcare solutions. A constructive model of a quartz crystal sensor (QCS) with a frequency output is considered and an algorithm for linearizing the QCS calibration characteristics is presented. An electrical QCS model is constructed and a numerical analysis of control characteristics in the presence of parasitic electrical connections arising from the practical implementation of the principle of capacitive control is carried out. A simulation model of a pulse oscillation sensor based on a QCS with capacitive control is presented and a numerical simulation of the stress-strain state of a corrugated membrane in COMSOL/Multiphysics is carried out. Examples of practical application of pulse wave QCS in systems of sphygmography for determining the parameters of the human cardiovascular system are given.

2.1. Motivation of the research

An important task of modern medicine is the effective diagnosis of arterial hemodynamics in order to identify the cardiovascular system (CVS) diseases at the early stages , to carry out preventive measures and timely treatment. In the diagnosis of CVS, methods of non-invasive measurement blood pressure (systolic, diastolic, mean) and heart rate are widely used. However, it is noted that in modern conditions the effectiveness of these methods is significantly limited, since their use does not fully provide the diagnosis of hemodynamics. It is emphasized that the "Prime time" has come for the widespread introduction of diagnostic methods, which are based on the

[2]***Authors:*** *Pidchenko Serhii, Taranchuk Alla*

study of the shape pulse oscillations in the main and peripheral arteries of a person [1].

Recently, the methods of applanation tonometry based on the pulse waveform analysis (PWA) and pulse wave velocity (PWV) analysis of the main and peripheral arteries of a person are becoming more and more widespread. In-depth PWA allows not only to study cardiac activity, but also to obtain a wide range of hemodynamic parameters of the central and peripheral circulatory system (blood flow parameters, peripheral resistance of the CVS, elastic-viscous properties of vascular walls) [2,3]. The PWA and PWV methods are of particular importance in the functional diagnosis of the initial stages of atherosclerotic changes [4]. Despite the fact that the causes of atherosclerosis remain not fully understood, it is believed that the initial stages of atherosclerosis occur already at a young age. Usually atherosclerosis reaches its clinical significance for persons of the older age group (over 50). Timely identification of risk factors and implementation of preventive measures can significantly slow down the progression of atherosclerosis, reduce the severity of its manifestations and prevent the occurrence of complications [5].

The widespread introduction of PWA is constrained by the lack of a unified concept of using methods for recording and processing pulse wave signals. This is due to a wide range of instruments for non-invasive recording of pulse wave signals, the data of which are sometimes difficult to compare with each other. Piezoresistive strain gauge sensors [6,7], optical sensors [8-9], acceleration sensors with a round film [10,11], piezoelectric sensors [12-14] are most widely used to register pulse wave signals. In [15], the efficiency of these pulsation sensors was assessed by comparing their stability and reproducibility of measurements, as well as their susceptibility to external factors: placement, contact strength and ambient light intensity (for an optical sensor). Comparison of four types of pulse wave sensors showed that in terms of stability and reproducibility of characteristics, an autonomous tonometer based on a piezoelectric sensor shows the best results. The worst results were obtained when recording a pulse wave using a system based on an optical sensor. It was revealed that the shape of the pulse wave signals significantly depends on the type of sensor and the features of its application [15].

It is possible to minimize the negative phenomena during registration of arterial pulse oscillations by improving the metrological characteristics of the pulsation sensor [16]. This makes it relevant to study the issues of constructing highly sensitive and highly stable sensors of pulse oscillations. The use of the sensors proposed by the authors for solving the problems of applanation tonometry will increase the efficiency of tools for non-invasive diagnostics of CVS and will contribute to the formation of a unified approach to the use of PWA in medical research.

2.2. Quartz crystal sensor design

The sensor based on a quartz resonator is a transducer with a frequency output. The resonant frequency of the transducer is controlled by changing the gap capacity between the excitation electrodes of the quartz piezoelectric element (PE).

The constructive scheme of quartz crystal sensor (QCS) is presented in Fig. 2.1. Under the action of a physical quantity (pressure *P*) the position of the moving electrode (membrane) changes. This leads to a change in the control capacitance *Ccontr* of the interelectrode excitation gap *x* of the quartz piezoelectric element transducer (Fig.2.1).

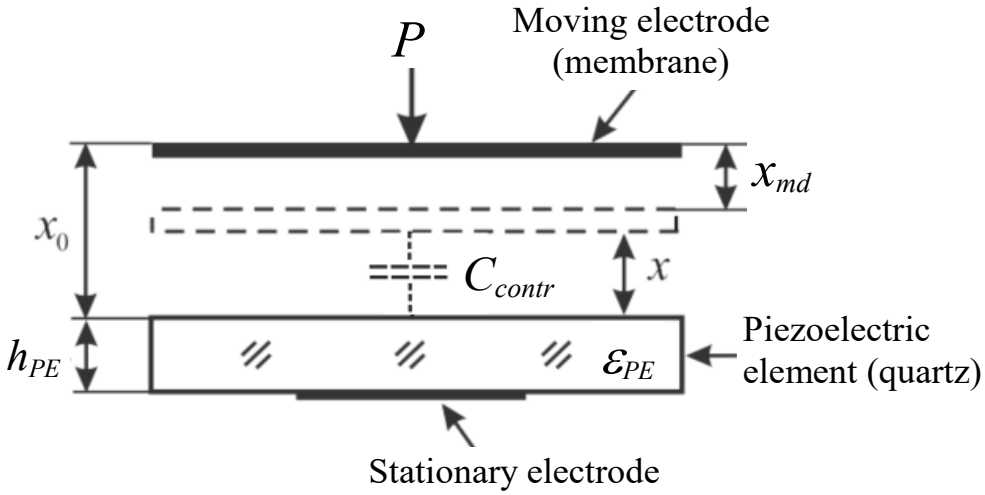

Figure 2.1 - Construction diagram of QCS

When PE is excited in the interelectrode gap x, the formula for the resonance frequency $f(x)$ of a QCS can be written as:

$$f(x) = f_0 \sqrt{1 + \frac{m}{1 + \frac{h_{PE}}{x \cdot \varepsilon_{PE}}}} \approx f_0 \left[1 + \frac{0.5m}{1 + \frac{h_{PE}}{x \cdot \varepsilon_{PE}}} \right], \quad (2.1)$$

where $x = x_0 - x_{md}$ is the current value of modulated interelectrode gap (MIG);

x_0 is the initial gap between the membrane and quartz piezoelectric element;

x_{md} is the membrane deflection at overpressure P;

f_0 is the nominal QCS frequency for $x_{md} = 0$;

m is the frequency coefficient of quartz PE;

h_{PE} and ε_{PE} is the thickness of the quartz piezoelectric element and its dielectric constant ($\varepsilon_{PE} = 4.5$).

Formula (1) for the output frequency of the sensor can be represented as

$$f(x) = f_0 + F(x), \; x \in [x_{\min}, x_0], \quad (2.2)$$

where $F(x)$ is the frequency calibration characteristic of the QCS.

The calibration characteristic $F(x)$ of QCS is described by a fractional-rational function:

$$F(x) = \frac{a_0 + a_1 x}{1 + a_2 x}, \quad (2.3)$$

where a_0, a_1, a_2 are the approximation coefficients, individual constants of the QCS.

A differential frequency is allocated to match the QCS output with digital devices $F_{dif}(x)$:

$$F_{dif}(x) = f_{het} - f(x) = (f_0 + F_{het}) - f(x) = F_{het} - F(x), \quad (2.4)$$

where f_{het} is the frequency of the local oscillator (heterodyne).

Next, we turn to the period $T(x)$ of the difference frequency signal (2.4) with (2.3):

$$T(x)=\left[F_{dif}(x)\right]^{-1}=\left[F_{het}-F(x)\right]^{-1}=\frac{\left(1+a_2x\right)}{F_{het}\left(1+a_2x\right)-\left(a_0+a_1x\right)}. \quad (2.5)$$

Analysis of the denominator (2.5) shows that the function $T(x)$ is transformed into a strictly linear function of the form

$$T_{lin}(x)=T_{0lin}+S_{lin}\cdot x \quad (2.6)$$

subject to the conditions

$$F_{het}=F_{het}^{(opt)}=\frac{a_1}{a_2}, \quad (2.7)$$

where $T_{0lin}=\left(\frac{a_1}{a_2}-a_0\right)^{-1}$ is the initial period for $x=x_0$; $S_{lin}=a_2\left(\frac{a_1}{a_2}-a_0\right)^{-1}$ is the steepness of the quartz crystal sensor conversion [16].

2.3. The electric model of quartz crystal sensor

The research studies the electrical characteristics of the QCS and considers its electric equivalent circuit (Fig. 2.2). The main element of QCS is a quartz resonator with equivalent dynamic inductance L_q, capacitance C_q, loss impedance R_q and parallel capacitance C_0. In series with the quartz resonator (QR), the control capacitance C_{contr} and (if necessary) inductance L_{ext} are included to increase the control range and improve linearity. Parasitic capacities $C_{par\,1}$ and $C_{par\,2}$ are also included in the equivalent electrical circuit, which significantly affects the characteristics of the QCS control. If excitation of a quartz resonator in a two-frequency (multi-frequency) mode is assumed, the equivalent circuit should be expanded by using additional dynamic circuits, the number of which should correspond to the number of additional modes of excited oscillations.

For the analysis of the equivalent electric circuit of the QCS, we use the method

proposed in [16, 17]. We find the conductivity between the points **a - b** of the equivalent scheme of the QCS (Fig. 2.2).

$$Y_{ab} = \frac{1}{Z'_{QR}} = \frac{1}{Z_q} + Y_{C0} = \frac{1}{R_q\left(1 + j\xi_q\right)} + j\omega C'_0 = \frac{1 - \tau'_C\xi_q + j\tau'_C}{R_q\left(1 + j\xi_q\right)}, \qquad (2.8)$$

where $Z_q = R_q\left(1 + j\xi_q\right)$ is the complex equivalent resistance of the series circuit L_q, C_q, R_q of the QR near the resonance; $Y_{C0} = j\omega C'_0 = j\omega\left(C_0 + C_{par1}\right)$ is the complex conductivity parallel connected C_0 and C_{par1}; $\xi_q = Q\left(\frac{\omega}{\omega_q} - \frac{\omega_q}{\omega}\right) \approx 2Q\delta_q$ – is the generalized detuning relative to the series resonance frequency; $\omega_q = 2\pi f_q = \left(L_q C_q\right)^{-0.5}$; $\delta_q = \frac{\omega - \omega_q}{\omega_q}$ is the relative frequency deviation, $Q = \sqrt{L_q / C_q} \cdot R_q^{-1}$ is the Q-factor of QR; $\tau'_C = \omega R_q C'_0$ – ratio of resistance to losses R_q and resistance of parallel capacitance $1/\omega C'_0$.

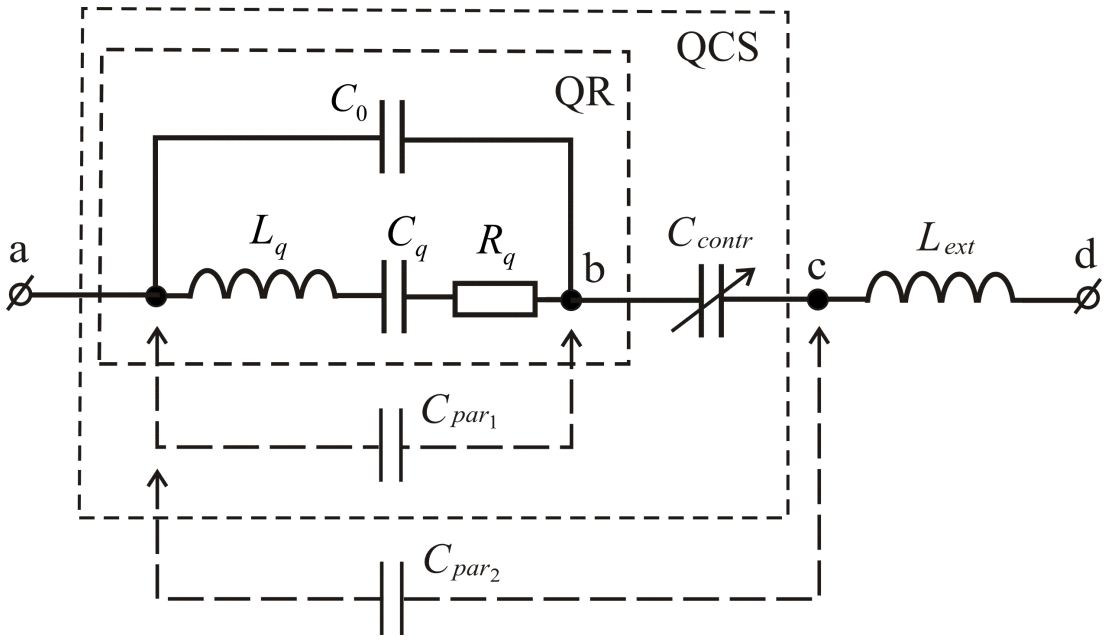

Figure 2.2 – Equivalent electric circuit of the QCS

The quality factor $M = \frac{1}{\tau'_C}$ (parallel Q) determines the activity of the quartz resonator when it is connected to the oscillator circuit ($M >> 1$).

The next step is to find the equivalent resistance of the serial connection Z'_{QR} and

the capacity of the control C_{contr}:

$$Z'_{QR_{contr}} = Z'_{QR} + Z_{C_{contr}} = \frac{R_q\left(1+j\xi_q\right)}{1-\tau'_C\xi_q+j\tau'_C} + \frac{1}{j\omega C_{contr}} = \frac{R_q\left(1-\xi_q T_1+jT_1\right)}{-T_2+j\left(\tau_{contr}-T_2\xi_q\right)}, \quad (2.9)$$

where $\tau_{contr} = \omega C_{contr} R_q$ is similarly to the τ'_0, the ratio of loss resistance R_q and the resistance of the control capacity $1/\omega C_{contr}$ is introduced by $T_1 = \tau_{contr} + \tau'_C$; $T_2 = \tau_{contr}\tau'_C$.

In turn, the conductivity between the points **a - c** will be determined as

$$\begin{aligned} Y_{ac} &= \frac{1}{Z_{\text{ac}}} = \frac{1}{Z'_{QR_{contr}}} + Y_{par_2} = \\ &= \frac{-T_2 + j\left(\tau_{contr} - T_2\xi_q\right)}{R_q\left(1-\xi_q T_1 + jT_1\right)} + j\omega C_{par_2} = \\ &= \frac{-\left(T_1\tau''_C + T_2\right) + j\left(\tau_{contr} + \tau''_C - \xi_q\left(T_1\tau''_C + T_2\right)\right)}{R_q\left(1-\xi_q T_1 + jT_1\right)} \end{aligned}, \quad (2.10)$$

where $\tau''_C = \omega R_q C_{par_2}$ is the resistance ratio of losses R_q and the resistance of the parasitic capacitance $1/\omega C_{par_2}$.

Then, the analytical expression for the complex equivalent resistance of the QRS electric circuit taking into account the elongation inductance L_{ext} (Fig. 2.2) will take the form:

$$\begin{aligned} Z_{QCS} &= Z_{ad} = Z_{ac} + j\omega L_{ext} = \\ &= R_q \times \left\{ \frac{1-\xi_q T_1 - \frac{1}{\tau'_L}\left(\tau_{contr} + \tau''_C - \xi_q T_3\right) + j\left(T_1 - \frac{T_3}{\tau'_L}\right)}{-T_3 + j\left(\tau_{contr} + \tau''_C - \xi_q T_3\right)} \right\} \end{aligned}, \quad (2.11)$$

where $\tau'_L = R_q/\omega L_{ext}$ is the resistance ratio of losses R_q and the resistance of the elongation inductance ωL_{ext}; $T_3 = T_1\tau''_C + T_2$.

Thus, the equivalent electrical resistance of the QCS Z_{QCS} (11) can be presented

in standard form

$$Z_{QCS}(j\omega) = \frac{A_1 + jB_1}{A_2 + jB_2}, \tag{2.12}$$

where $A_1 = R_q\left(1 - \xi_q T_1 - \frac{T_4}{\tau'_L}\right)$; $B_1 = R_q\left(T_1 - \frac{T_3}{\tau'_L}\right)$; $A_2 = -T_3$; $B_2 = T_4$; $T_4 = \tau_{contr} + \tau''_C - \xi_q T_3$.

Analysis (2.12) allows to determine the basic electrical parameters of the piezoresonance oscillatory system of the QCS: the frequencies of the serial resonance f_r (ω_r) and the parallel resonance (antiresonance) f_{par} (ω_{par}); equivalent quality factor Q_{eq} (fixing ability); equivalent series resistance (ESR) and others. So, equating the imaginary part $\mathrm{Im}\left(Z_{QCS}(j\omega)\right)$ of $Z_{QCS}(j\omega)$ (2.12) to zero $\left(B_1(\xi_q)A_2(\xi_q) - A_1(\xi_q)B_2(\xi_q) = 0\right)$, we obtain an equation for the generalized detuning ξ_q, which allows us to determine the resonance frequencies of QCS:

$$k_2 \cdot \xi_q^2 + k_1 \cdot \xi_q + k_0 = 0, \tag{2.13}$$

where $k_2 = T_3\left(T_1 - \frac{T_3}{\tau'_L}\right)$;

$k_1 = \left(\frac{2}{\tau'_L}T_3 - T_1\right)\left(\tau_{contr} + \tau''_C\right) - T_3$;

$k_0 = \tau_{contr} + \tau''_C + T_1T_3 - \frac{1}{\tau'_L}\left(\left(\tau_{contr} - \tau''_C\right)^2 + T_3^2\right)$.

Having distinguished the real part $\mathrm{Re}\left(Z_{QCS}(j\omega)\right)$, we obtain the equivalent series (ESR) and parallel (EPR) resistance of the QCS:

$$\mathrm{ESR} = \mathrm{Re}\left(Z_{QCS}(j\omega)\right)\Big|_{\omega = \omega_r} \tag{2.14}$$

and

$$\mathrm{EPR} = \mathrm{Re}\left(Z_{QCS}(j\omega)\right)\Big|_{\omega = \omega_{par}}, \tag{2.15}$$

where $\mathrm{Re}\left(Z_{QCS}(j\omega)\right)=\dfrac{A_1(\omega)\cdot A_2(\omega)+B_1(\omega)\cdot B_2(\omega)}{\left(A_2(\omega)\right)^2+\left(B_2(\omega)\right)^2}$ is the real part of the complex equivalent resistance $Z_{QCS}(j\omega)$.

One of the most important parameters of the oscillating system is its fixing ability σ, which is directly related to the equivalent quality factor Q_{eq}:

$$\sigma=\omega\left|\frac{d\phi(\omega)}{d\omega}\right|_{\omega=\omega_r}\approx 2Q_{eq}, \tag{2.16}$$

where $\dfrac{d\phi(\omega)}{d\omega}$ is the steepness of the phase-frequency characteristic QRS $\phi(\omega)$ near resonance.

To determine $\phi(\omega)$, we represent the equivalent complex resistance of the QCS (2.12) in an exponential form:

$$Z_{QCS}(j\omega)=\left|Z(\omega)\right|\exp^{j\phi(\omega)}, \tag{2.17}$$

where $\phi(\omega)=\phi_1(\omega)-\phi_2(\omega)=arctg\left(\dfrac{B_1}{A_1}\right)-arctg\left(\dfrac{B_2}{A_2}\right)$.

2.4. Numerical analysis of the quartz oscillatory system with capacitive control

The research analyzes the characteristics of the oscillatory system QCS on the basis of a flat quartz piezoelectric element with the parameters: AT-cut (Ø 12 mm); frequency of the main resonance $f_q=10.009987$ MHz for Q factor 103000 and resistance $R_q=24$ Ohm; parallel capacity C_0 =3.5 pF [16].

Fig. 2.3a,b present the curves of the frequency of series $\Delta F_r=f_r-f_q$ and $\Delta F_{par}=f_{par}-f_q$ parallel resonances with a change in the control capacitance C_{contr} and parasitic capacitance $C_{par\,1}$, Fig. 2.4a,b present the curves of the equivalent series

loss resistance ESR and Q-factor $q = Q_{eq}/Q$, respectively.

The analysis of the obtained data confirms the high efficiency of control with the use of a series-connected capacity C_{contr}. Control characteristics (Fig. 3a) are highly nonlinear. This requires the use of method (2.2) - (2.7) to linearize the sensor conversion characteristics. At the same time, at the edges of the characteristic $\Delta F_r(C_{contr})$ it is possible to distinguish the sections with weak nonlinearity, for example, for the $C_{contr} \in [1; 3]$pF and $C_{contr} \in [17.5; 27.5]$pF ranges. The average value of the control slope in the first case is 1000 Hz/pF, and in the second case – 50 Hz/pF (Fig. 2.3a, Curve 1).

The use of the control range $C_{contr} \in [1; 3]$ pF is more preferable because of the extremely high control slope, however, a sharp (almost an order of value) increase in the series resistance of the EPR is observed (Fig. 2.4a, Curve 1).

Compensation (to some extent) of the negative effect of the presence of parasitic capacitance C_{par1} can be achieved by including the extension inductance L_{ext} (Fig. 2.2), which increases the frequency range of control characteristics, using a frequency domain lower than f_q (Fig. 2.5a; $C_{contr} \in [17.5; 30]$pF). The value of the inductance L_{ext} is chosen so that the inductive reactance $\omega_q L_{ext}$ compensates for the capacitive control component $1/\omega_q C_{contr}$.

It should be noted that at the same time, for relatively large values of $C_{par1} \in [2.5; 5]$ pF, the equivalent resistance of ESR also significantly increases in accordance with Fig. 2.4a.

The situation is different when controlling QCS by modulating of interelectrode excitation capacitance gap (Fig. 2.5b). Since the parallel parasitic capacitance C_{par2} that occurs, in this case, is included through the control capacitance C_{contr} (Fig. 2.2), it has a significantly lower effect on the characteristic of the QCS control, the steepness S_{contr} of which approaches the maximum possible values (Fig. 2.5b, Window 2, Curves 1-3).

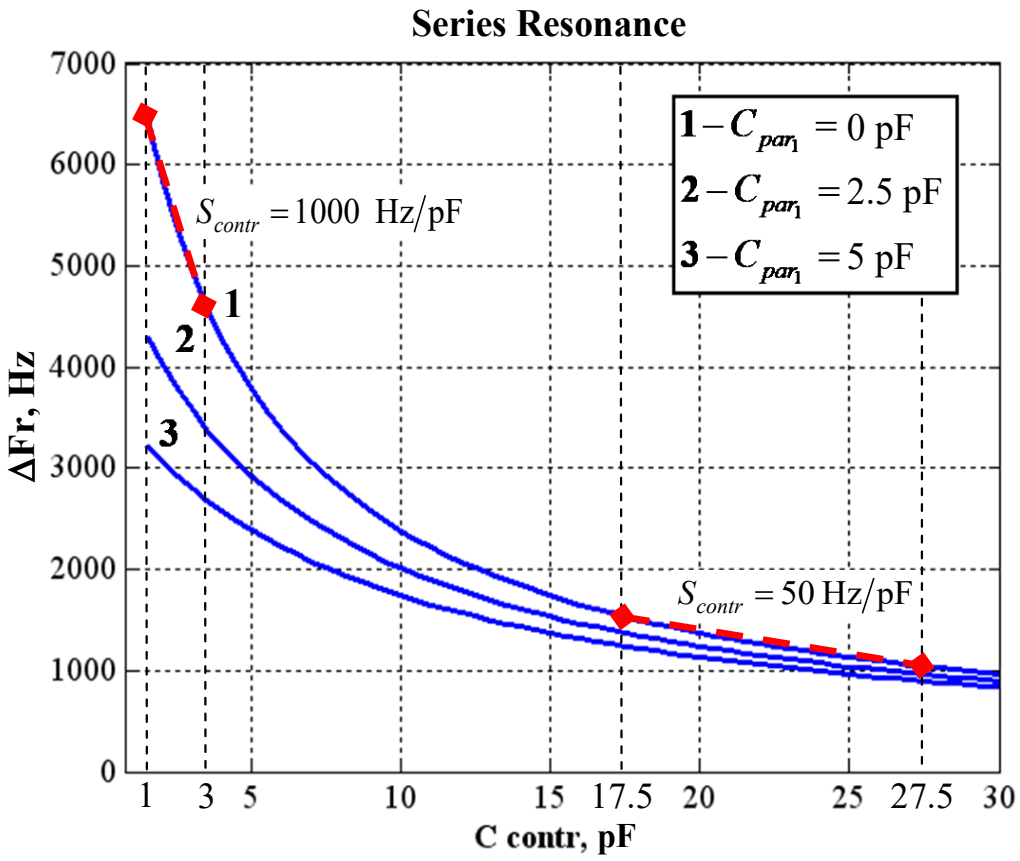

(а)

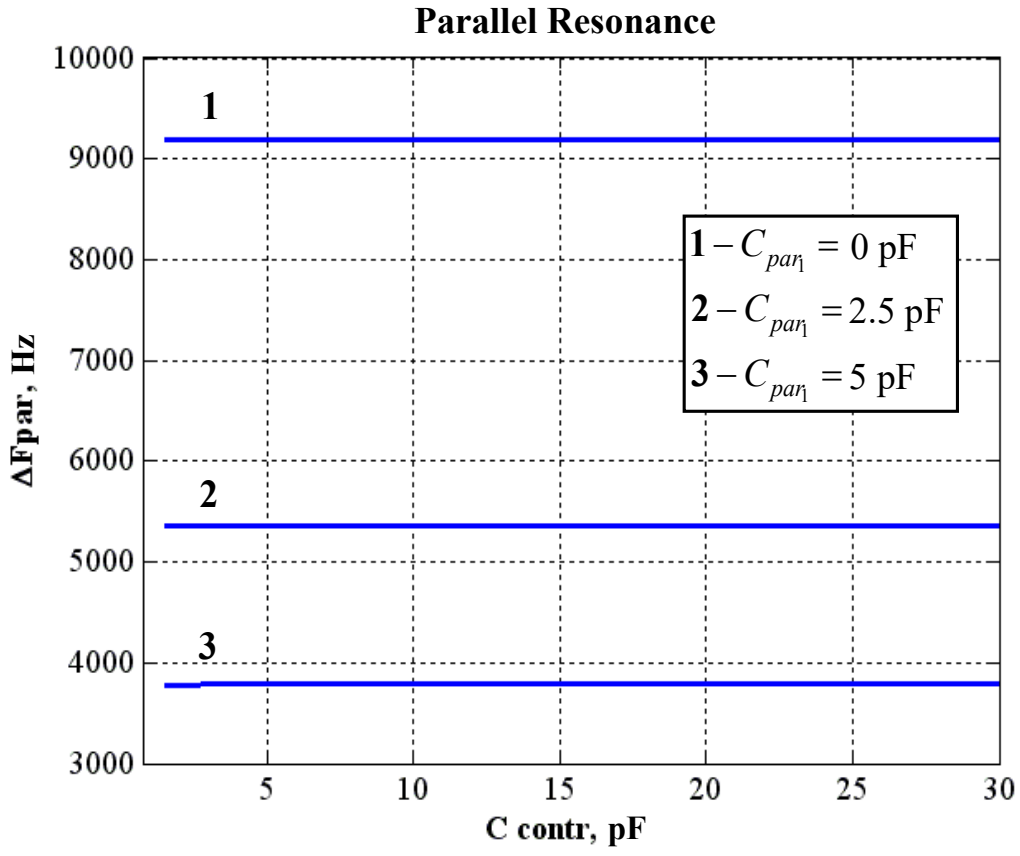

(б)

Figure 2.3 – Series ΔF_r – (a) and parallel ΔF_{par} – (b) resonances of the QRS oscillation system as a function of the control capacitance C_{contr} when the parasitic capacitance C_{par} changes

At the same time, the variations in the values of the series resonance ΔF_r within $C_{contr} \in [1.5;\ 30]$ pF are as close as possible to the dependence shown in Fig. 2.3a (Curve 1).

2.5. Numerical simulation of a strained-deformed state of a corrugated membrane

Numerical simulation of the stress-deformed state of a metal corrugated membrane (CM) is performed on the basis of the finite element method by solving the multifunctional electromechanics problem in the system of physical modeling of COMSOL Multiphysics.

The main elements of the three-dimensional (3D) model of the quartz pressure sensor (Fig. 2.6) are a piezoelectric element, which is located on special quartz holders and a corrugated membrane that is rigidly fixed in the contour. The piezoelectric element, which is applied in the center by the electrode and CM, forms a quartz resonator controlled by excess pressure ΔP. The resonance frequency of the sensor depends on the capacity C_{contr} of the excitation gap, which is formed between the PE and the central part of the corrugated membrane (Fig. 2.1).

For linear conditions (small displacements), COMSOL Multiphysics software formalizes a stress-strain state using the equation:

$$1.\ \boldsymbol{\sigma} = \mathbf{D}\boldsymbol{\varepsilon}, \tag{2.18}$$

where $\mathbf{D}$ - a matrix of elasticity, vectors of mechanical stresses and deformations – $\boldsymbol{\sigma} = \left[\sigma_x\ \sigma_y\ \sigma_z\ \tau_{xy}\ \tau_{yz}\ \tau_{xz}\right]^{\mathrm{T}}$ and $\boldsymbol{\varepsilon} = \left[\varepsilon_x\ \varepsilon_y\ \varepsilon_z\ \varepsilon_{xy}\ \varepsilon_{yz}\ \varepsilon_{xz}\right]^{\mathrm{T}}$ consist of three normal components $\sigma_x, \sigma_y, \sigma_z$ and $\varepsilon_x, \varepsilon_y, \varepsilon_z$ those three tangents (in symmetry $\tau_{xy} = \tau_{yx}$, $\tau_{xz} = \tau_{zx}$, $\tau_{yz} = \tau_{zy}$, $\varepsilon_{xy} = \varepsilon_{yx}$, $\varepsilon_{xz} = \varepsilon_{zx}$, $\varepsilon_{yz} = \varepsilon_{zy}$) component $\tau_{xy}, \tau_{yz}, \tau_{xz}$ and $\varepsilon_x, \varepsilon_y, \varepsilon_z$.

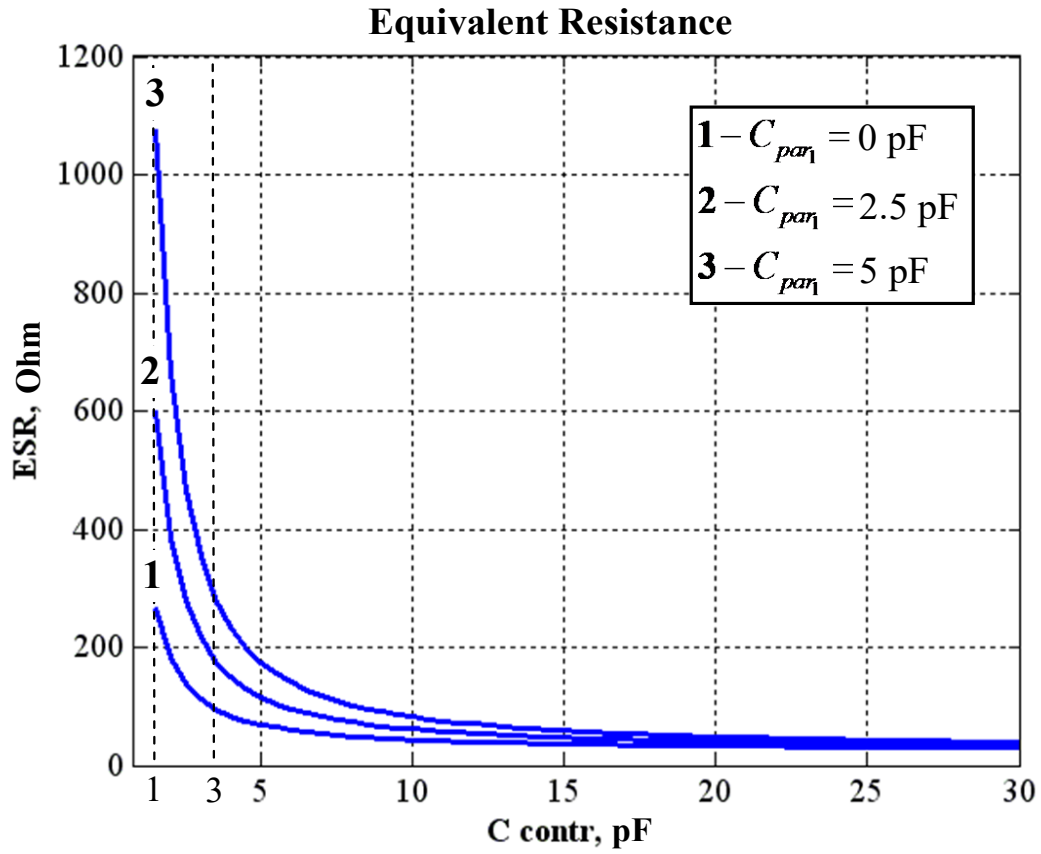

(a)

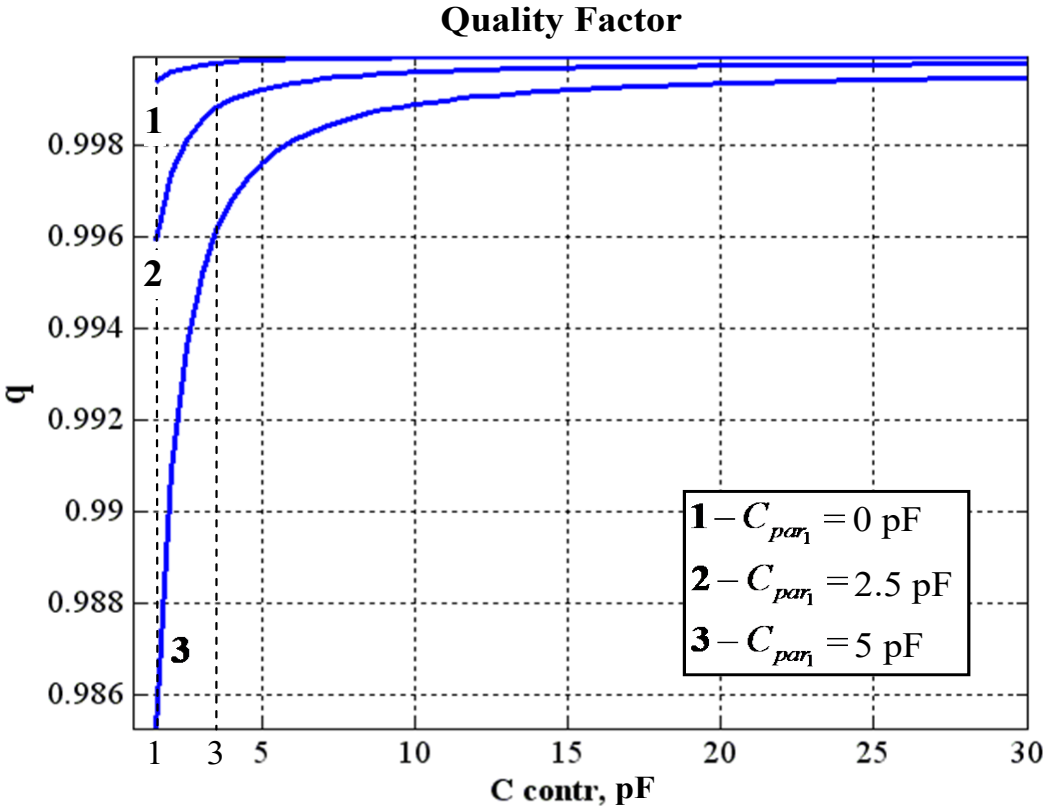

(б)

Figure 2.4 – Dependences of the equivalent series resistance (ESR) (a) and Q-factor *q* (b) of the QCS oscillation system as a function of the control capacitance C_{contr} when the parasitic capacitance C_{par1} changes

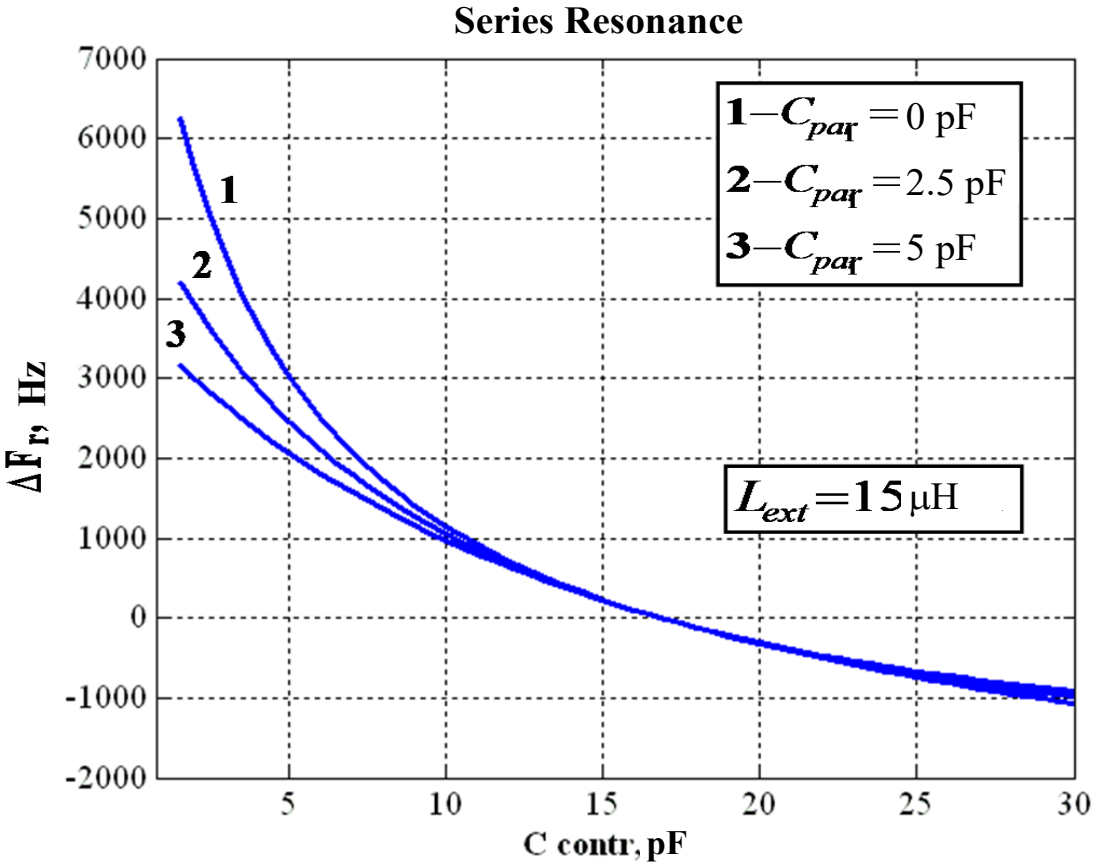

(a)

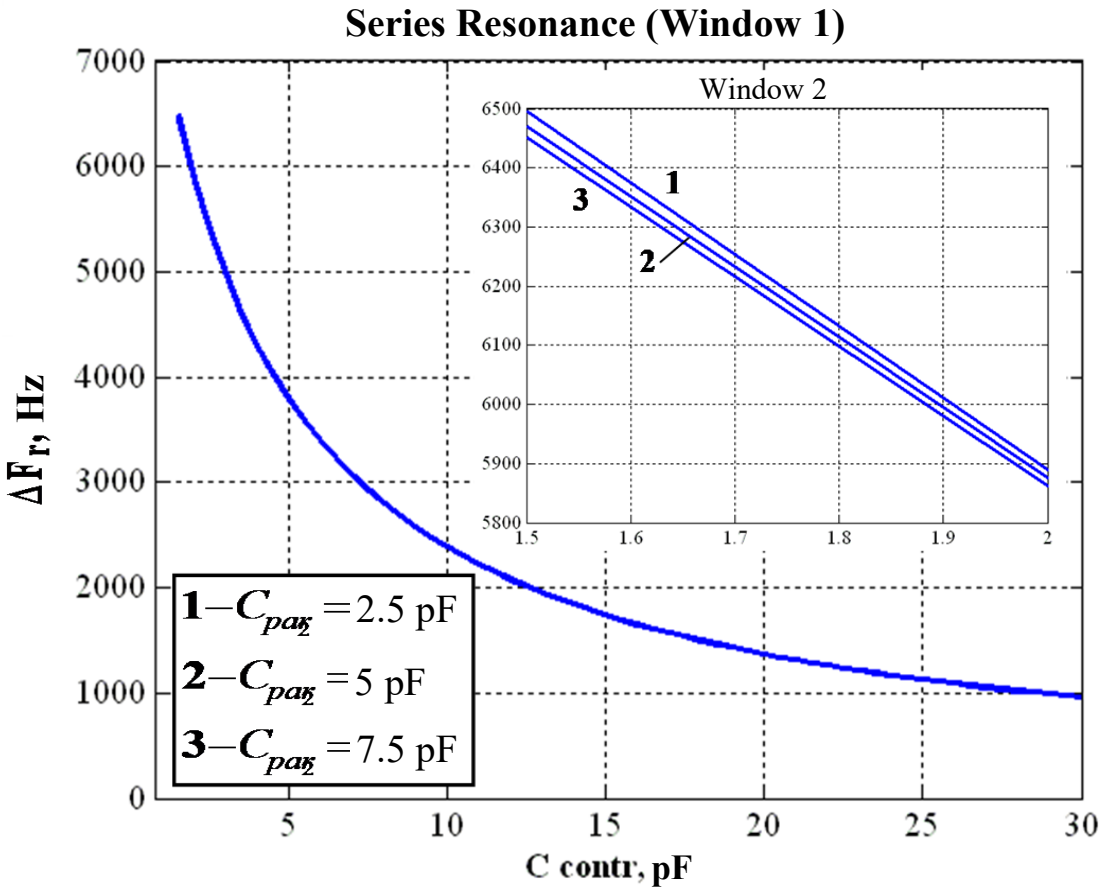

(б)

Figure 2.5 – Characteristicsof the QCS as a function of the control capacitance C_{contr} with inductance L_{ext} enabled (a) and parasitic capacitance C_{par1} change (b)

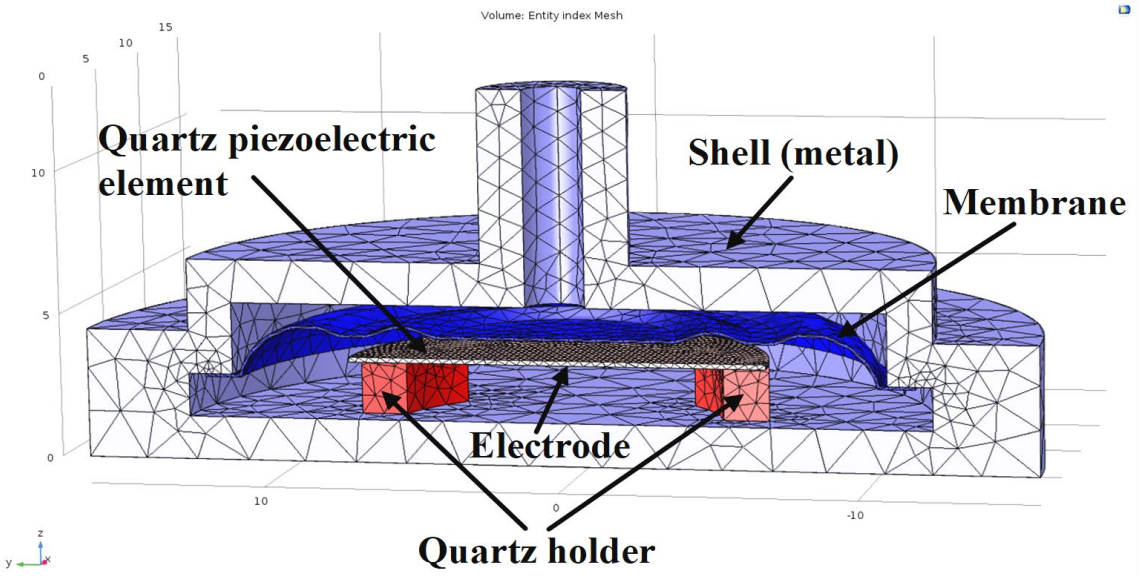

Figure 2.6 – Three-dimensional (3D) model of the excess pressure sensor (COMSOL Multiphysics)

In an isotropic interpretation, the matrix of elasticity **D** is defined as

$$\mathbf{D} = A \times \begin{bmatrix} 1-\mu & \mu & \mu & 0 & 0 & 0 \\ \mu & 1-\mu & \mu & 0 & 0 & 0 \\ \mu & \mu & 1-\mu & 0 & 0 & 0 \\ 0 & 0 & 0 & \frac{1-2\mu}{2} & 0 & 0 \\ 0 & 0 & 0 & 0 & \frac{1-2\mu}{2} & 0 \\ 0 & 0 & 0 & 0 & 0 & \frac{1-2\mu}{2} \end{bmatrix}, \quad (2.19)$$

where $A = \frac{E}{(1+\mu)(1-2\mu)}$; E – Young's module; μ – Poisson coefficient.

When applied pressure P, which exceeds the atmospheric pressure, the deflection of the membrane occurs (Fig. 2.7), resulting in a decrease in the size of the gap x_{md} between the central surface of the PE and the working surface of the CM. It can be seen that the membrane gets a variable deflection. The centre of the membrane has the greatest displacement and the its periphery has the smallest one (Fig. 2.7).

To study the characteristics of a piezoresonance overpressure sensor with a variable interelectrode excitation gap, its numerical simulation was carried out in COMSOL Multiphysics (materials temperature – 20°C) (Fig. 2.8,2.9). The results of the simulation model confirm the high linearity of the deflection characteristics of the CM in the range of excess pressure $\Delta P \in [0;\ 40000]$ Pa or $\Delta P \in [0;\ 300]$ mm Hg. The membrane of the "soft" AERIS 1345 ("BrB2") alloy provides nearly 50% more sensitive than 36NHTY membrane. However, its maximum deflection goes beyond the permissible range $x_{md} \in [0;70\ \mu m]$, which must be taken into account when constructing pressure sensors of this type (Fig. 2.8).

Accordingly, the capacity C_{contr} of the interelectrode gap for overpressure $\Delta P > 32500$ Pa (Fig. 2.9) is beyond the limits of the values $C_{contr} \in [1.5;\ 30]$, which are necessary for the effective control of QCS (Fig. 2.3) [18].

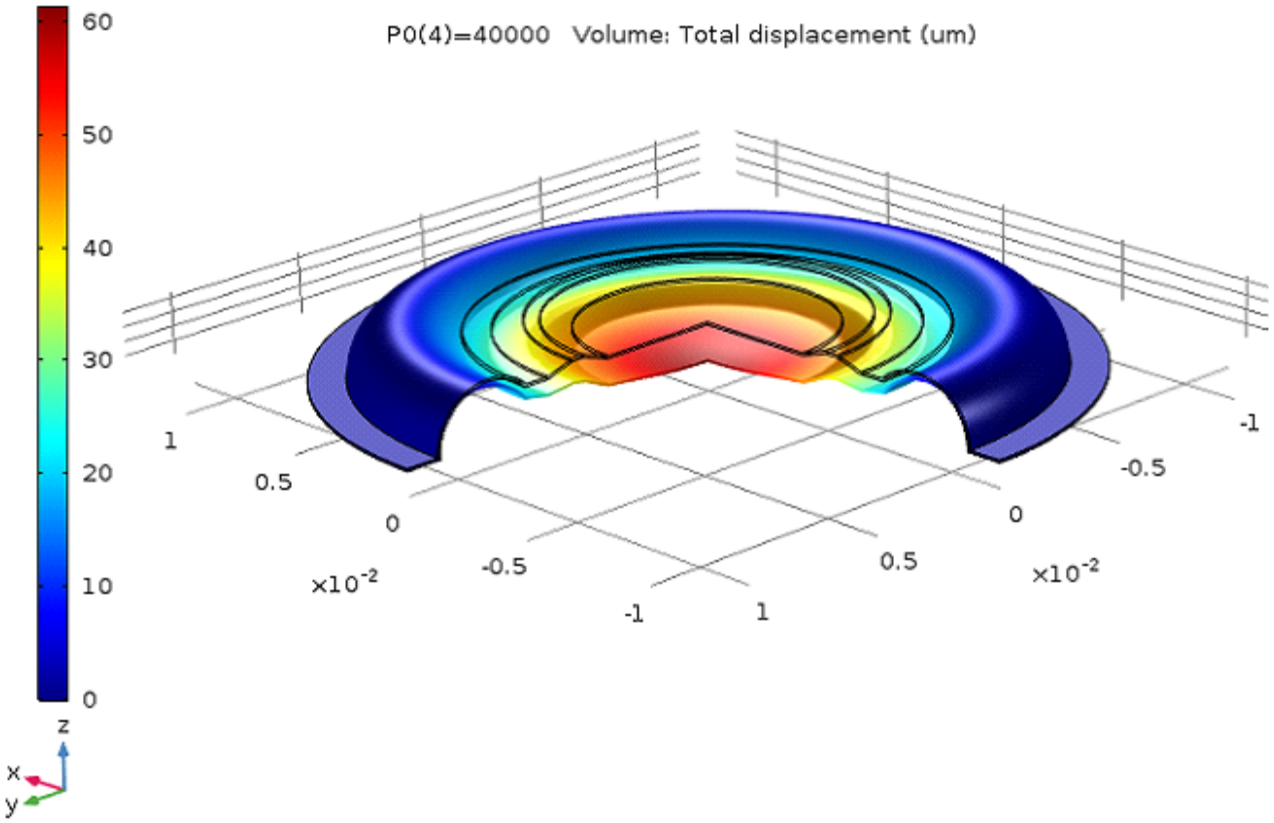

Figure 2.7 – Three-dimensional (3D) model of the excess pressure sensor (COMSOL Multiphysics)

2.6. Practical implementation of pressure sensors based on capacitive controlled quartz resonators

The practical implementation of quartz pulse wave sensors with capacitive control is considered in [19, 20]. In this application, QCS (Fig. 2.10 and Fig. 2.11) are the basis of a multichannel system of sphygmography for studying the parameters of the human cardiovascular system.

A flat piezoelectric element (**PE**, Fig. 11) of the AT-cut (Ø 12 mm) with an electrode in the central region is used to construct pulse wave QCS-'s. The nominal frequency of the QCS is $f_q = 10.000$ MHz. The control of the interelectrode gap of the PE excitation under pressure is carried out using a CM (Ø 24 mm, 36NHTY). The profile and diameter CM (**M**, Fig. 2.10) are chosen in such a way that they can minimize the constructive parasitic capacitance C_{pan} and bring the QCS sensitivity closer to the maximum possible values (Fig. 2.3a).

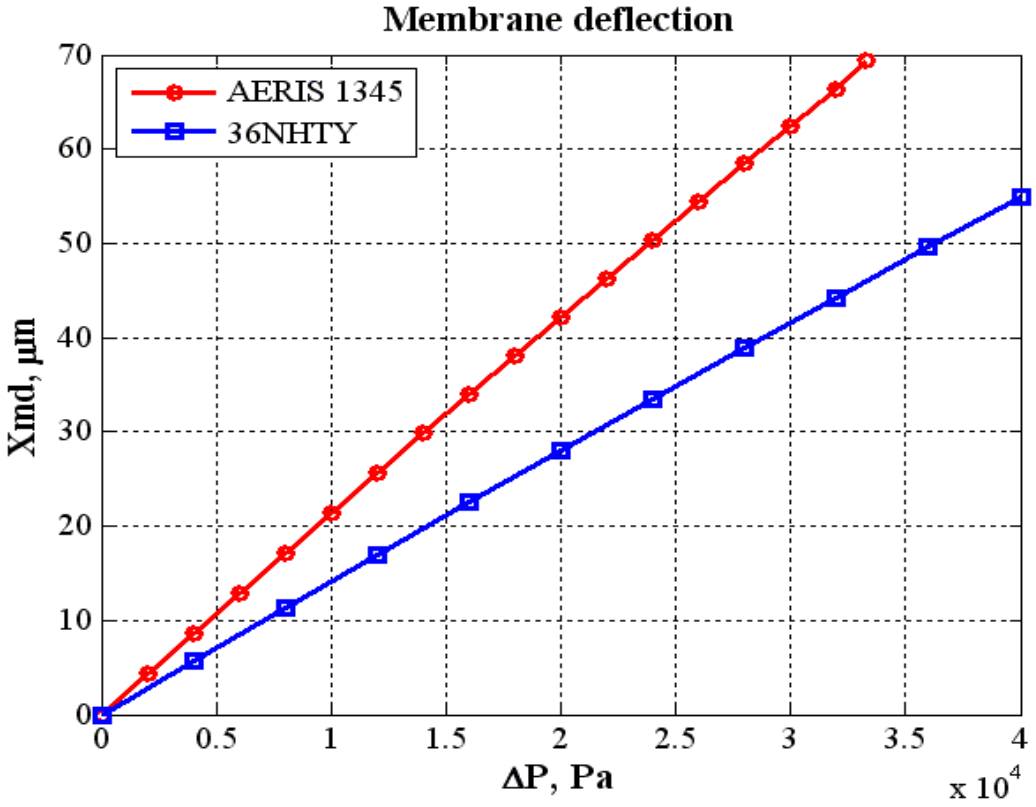

Figure 2.8 – Dependences of the membrane deflection $x_{md,max}$ on the value of the applied pressure ΔP

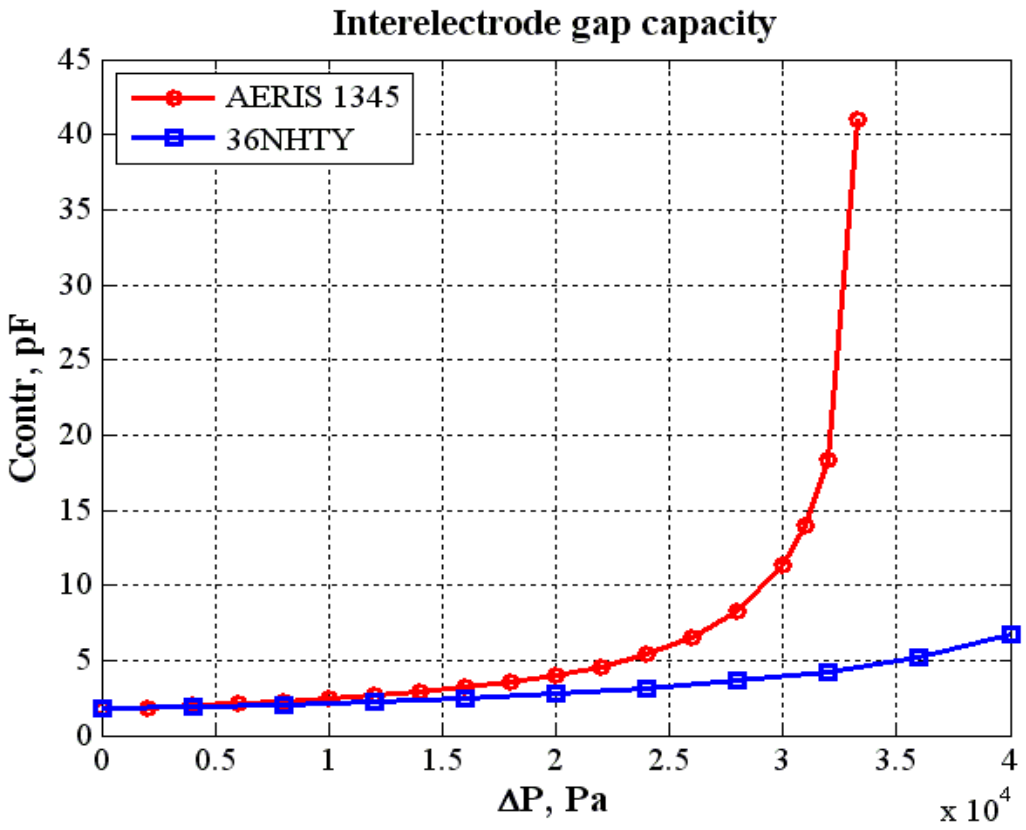

Figure 2.9 – Dependences of the interelectrode gap capacity C_{contr} on the value of the applied pressure ΔP

The electronic excitation circuit QCS (**EC**, Fig. 2.10) uses the Colpitts oscillator structure [21] and is located in close proximity to the PE - CM assembly. This allows the design parasitic capacitance C_{par_2} to be minimized (Fig 2.5b).

The structural diagram of the QCS (Fig. 2.1) allows placing all the elements of the sensor in a metal shell, which is connected to the zero potential of the circuit. The metal shell (Fig. 2.10, Fig. 2.11) is a shield from external electric fields, which significantly increases the noise immunity of the sensor and the stability of its characteristics.

To increase the efficiency of the post-processing of signals from the IPS sensors in the frequency domain, it is advisable to use the algorithms described in [22].

Typical characteristics of a quartz pressure sensor for recording pulse oscillations on the human carotid artery (Fig. 2.10) are presented below.

1. Pressure range ……..……...$[0;40]$kPa.

2. Resolution in the range of applied pressure:

– for small pressure, less than 1.5 kPa …… 1.2 Pa;

– for maximum pressure, not worse ..…… 3.0 Pa.

3. Full change-over of frequency, not less than …… 5.5 kHz.

4. The value of hysteresis after maximum load, not more than …… 2 Hz.

5. The basic error of measurement the surplus pressure, not more than ..... 0.15%.

6. Overall dimensions:

– diameter.....Ø 38 mm

– length……..…30 mm

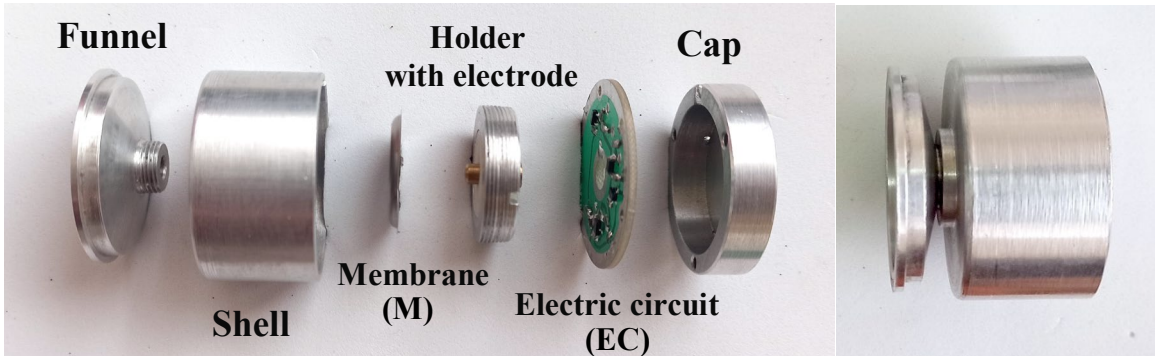

(a) **(b)**

Figure 2.10 – Structural elements (a) and appearance (b) of a capacitive-controlled quartz crystal sensor

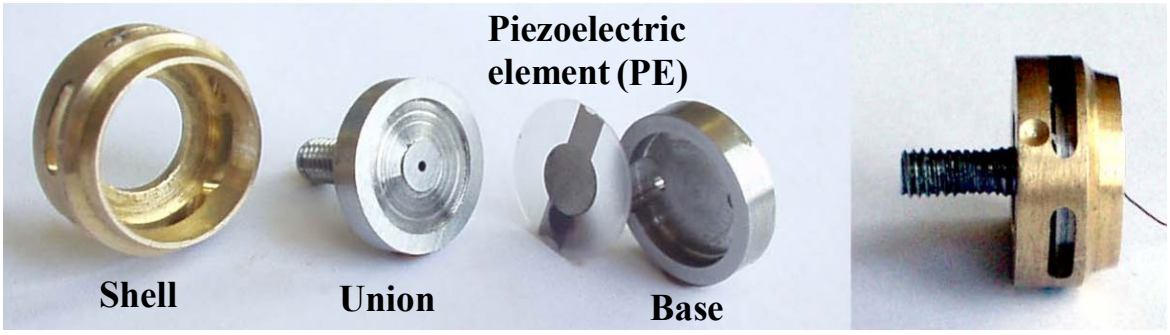

(a) **(b)**

Figure 2.11 – Structural elements (a) and appearance (b) of a capacitive-controlled quartz crystal sensor with resonating membrane

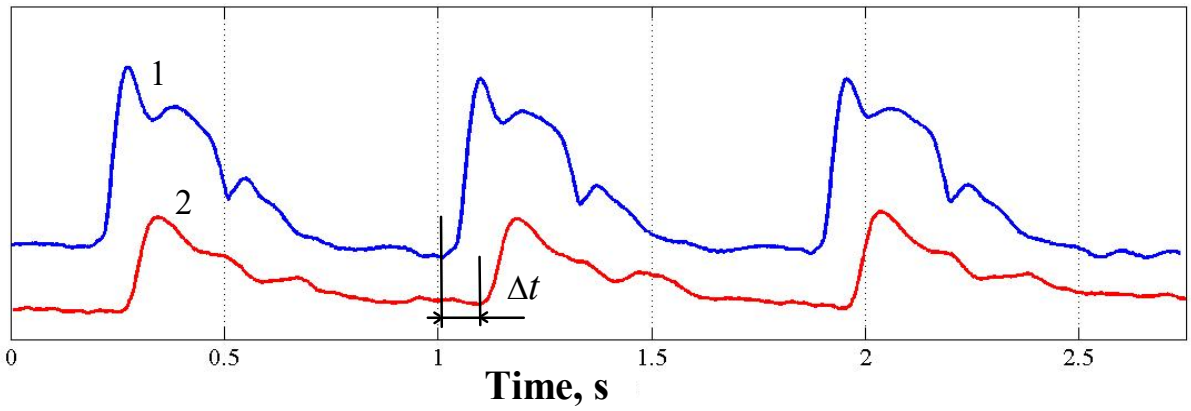

Figure 2.12 – Normal pulse wave signals on the carotid artery (1) and radial artery (2), recorded by a quartz crystal sensor with capacitive control

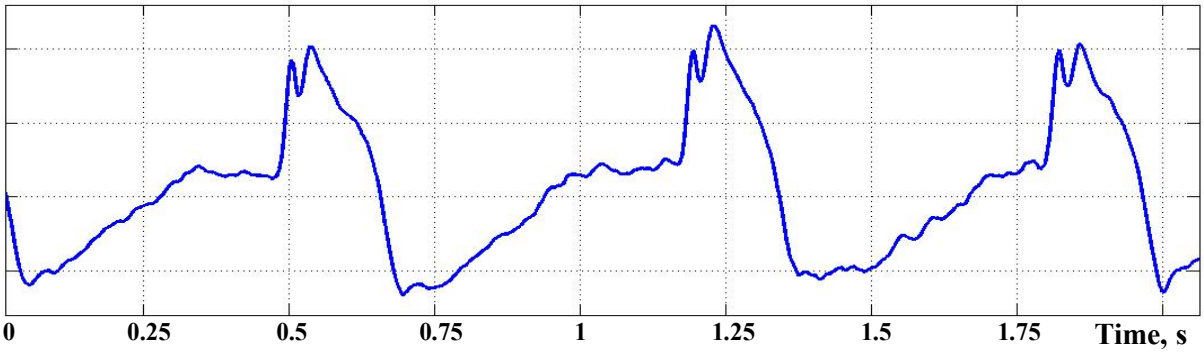

(a)

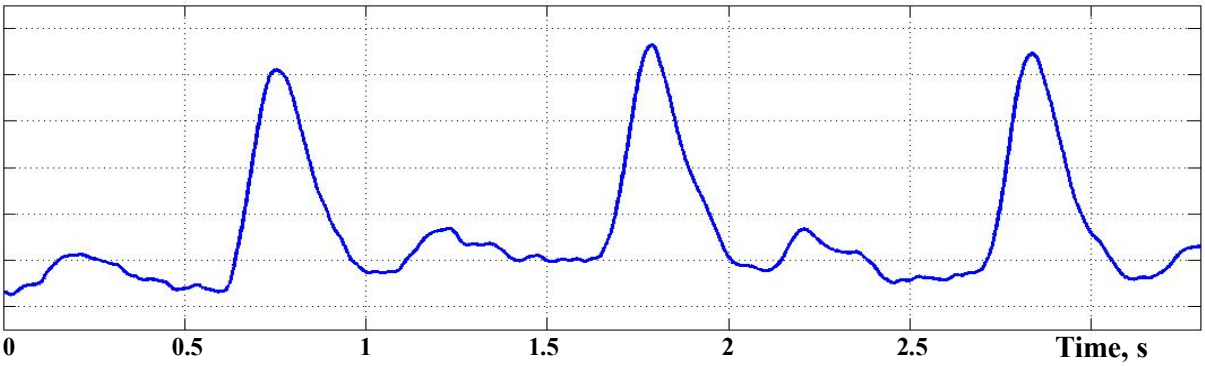

(b)

Figure 2.13 – Pulse wave signals of the carotid (a) and radial (b) arteries, recorded by a quartz crystal sensor with capacitive control in patients with diagnosed aortic insufficiency and mitral valve prolapse, respectively

Fig. 2.12 and Fig. 2.13 show the examples of the pulse wave signals of the carotid and radial arteries recorded by a quartz sensor with capacitive control of patients without diagnosed CVS diseases (Fig. 2.12) and diagnosed CVS diseases (Fig. 2.13). The presented pulse wave signals confirm the high efficiency of using QCS with capacitive control to solve diagnostic problems of CVS applanation tonometry [19, 20].

Conclusions

Analysis of the electrical characteristics of the pulse wave QCS confirms the high efficiency of the selected capacitive control method. At the same time, the most rational is the use of movable membrane-type electrodes, which minimizes parasitic structural electrical connections. This brings the control characteristics of QCS closer to potential dependencies.

It is necessary to ensure high stability of oscillations in conditions of a significant decrease in the activity of the quartz resonator to use the full frequency tuning range of the QCS. For this reason it is recommended to use quartz crystal oscillators built according to filter circuits.

A quartz pulse wave sensor with frequency output matches well with digital post-processing devices and does not require additional analog-to-digital conversion. The stated principles of QCS construction are also applicable to Quartz & MEMS technologies.

The combination of high resolution capacitive membrane sensors and high stability of the quartz crystal sensors parameters ensures high reliability of the recorded data. This implies the effective use of pulse wave QCS for healthcare solutions, in particular for detecting pathological changes in the work of the heart and the state of blood vessels at an early stage of the disease.